*Silvester Kolic[1], Marina Džomba[1], Marija Mitrovic[2], Nevenka R. Elezovic[3]**

[1]SIGMA LLC, Crvenka, Republic of Serbia, [2]University of East Sarajevo, Faculty of Technology Zvornik, Zvornik, Republic of Srpska, Bosnia and Herzegovina, [3]University of Belgrade Institute for Multidisciplinary Research-National institute of the Republic of Serbia, Belgrade, Serbia

Scientific paper
ISSN 0351-9465, E-ISSN 2466-2585
https://doi.org/10.62638/ZasMat2106



Zastita Materijala 67 ()
(2026)

Application of a physics informed neural network to optimization of chlorine production by membrane-less electrolysis

ABSTRACT

This paper shows how a physics-informed neural network (PINN) can connect Faraday's balance, changing electrolyte conductivity, and experimental data in a model of available-chlorine production. First, a steady-state component balance yields a baseline linear relation between concentration and active electrode length. The paper then shows why assuming constant current density overestimates outlet concentration in a longer cascade electrolyzer: electrolyte conductivity declines during conversion. Six Aqualor H measurements are used to derive the correlation $\kappa(C) = 49.300 - 0.77148 \cdot C^{1.322} \cdot e^{-0.10216 \cdot C}$*, inspired by semiempirical models of free-ion concentration and mobility. The PINN approximates the spatial concentration profile and learns by reducing the differential-equation residual and inlet-condition error. The plots show approximate agreement between the PINN and theoretical model for the short H25 pilot electrolyzer, while experimental yield is lower because of vessel-volume effects. For the H1000, the PINN follows the experimental profile more closely than the constant-current theoretical model. The enhanced model uses the composite conductivity correlation; numerical solution of its governing equation gives an outlet concentration of about 9.48 g/L for the adopted parameters, versus 10.10 g/L from the baseline model and 9.4 g/L in the displayed experimental series.*

***Keywords**: PINN; artificial intelligence; available chlorine; membraneless electrolysis; Faraday's law; electrolyte conductivity; Aqualor H.*

1. INTRODUCTION

Electrochemical technologies provide a direct connection between electrical energy and chemical production, with performance governed by electrode kinetics, ionic transport and reactor design [1, 2]. Chlor-alkali technology is an established industrial application [3, 4], while chlorine and hypochlorite are widely used in disinfection and water treatment [5]. Dimensionally stable anodes, developed by Beer, made durable catalytic oxide electrodes available for industrial service [6]. Their behaviour in chlorine and oxygen evolution remains central to electrochemical selectivity and energy demand [7].

On-site electrochemical generation of available chlorine offers an alternative to transporting and storing externally manufactured disinfectants [8, 9]. Dilute sodium chloride solutions can be converted into chlorine-containing oxidants at the point of use, although energy consumption, electrode durability and product quality must be evaluated for each installation.

Corresonding author: Nevenka Elezovic
E-mail: nelezovic@tmf.bg.ac.rs
Paper received: 22. 10. 2026.
Paper accepted: 28. 10. 2026.

Electrochemical environmental technologies also include ferrate generation [10], electro-coagulation [11], and direct or mediated oxidation of organic pollutants [12, 13]. These processes provide broader context for local electrically driven treatment, but their mechanisms and products differ from those of HLOROGENelectrochlorination [14].

Available-chlorine production depends on electrode material, current density, brine composition, temperature and hydrodynamics [1–4, 8]. Competing chlorine and oxygen evolution reactions influence current efficiency [7], and the acid dissociation equilibrium of hypochlorous acid determines the pH-dependent distribution between HOCl and OCl^- [15]. Consequently, achieving a specified chlorine concentration does not by itself establish disinfection performance or compliance with application-specific product requirements [5, 9]. The present study concerns available chlorine expressed as Cl_2 equivalent; it does not model chlorine dioxide production.

Mathematical modelling links electrochemical reaction rates to transport, cell voltage and production capacity [1, 3, 4]. For renewable-powered operation, this process description must

also be coupled to converter losses, auxiliary consumption and the time-dependent availability of electricity. The existing HLOROGENH25 and H1000 information supplies a starting point for the reactor model [16], while the Aqualor H measurements and supplied PINN implementation support the conductivity-dependent extension [17, 18]. The literature conductivity models used to motivate the empirical correlation are identified separately [19–21]. Thus, development of dimensionally stable electrodes has enabled more selective electrochemical production of available chlorine at the point of use. Such in situ production aligns capacity with demand, reduces storage needs, provides a fresh, high-purity product, often eliminates post-treatment of the finished solution, simplifies maintenance, lowers energy consumption, and limits the handling of hazardous chemicals [16]. HLOROGEN technology uses dilute NaCl solution and produces approximately 9–10 g/L of chlorine equivalent at the outlet of commercial HLOROGEN units.

This paper aims to demonstrate the value of artificial intelligence in electrolysis modeling through a concrete PINN implementation. Its advantage is the ability to determine the concentration profile while enforcing the material balance, rather than merely interpolating measured points. The baseline balance and experiment come from the HLOROGEN development documentation [16], the composite conductivity relation from a separate Aqualor H analysis [17], and the implementation of the enhanced PINN model from subsequent HLOROGEN development work.

The novelty of this research is the application-specific coupling of the electrochemical balance with measured conductivity changes, rather than the PINN method itself. Classical artificial neural networks (ANNs) typically learn input–output relationships by minimizing prediction errors against training data, without explicitly enforcing electrochemical balances or transport equations. Physics-informed neural networks (PINNs), by contrast, incorporate governing equations and boundary conditions into the training objective, potentially reducing dependence on labelled measurements and promoting physically consistent predictions. However, these advantages depend on the accuracy of the underlying physical model; PINNs can inherit errors from omitted mechanisms, require careful selection of loss weights and training points, and encounter convergence difficulties and substantial computational costs. Neither improved extrapolation nor greater accuracy than conventional numerical methods is therefore guaranteed. Within this established methodological framework, the contribution of the present study is the integration of a Faraday-based material balance with an experimentally calibrated conductivity–concentration relationship in a PINN representation of available-chlorine production in membrane-less electrolyzers. This formulation accounts for the downstream reduction in local current density that is neglected by the constant-current baseline model, while comparison of the H25 and H1000 configurations helps distinguish conductivity-related effects from discrepancies associated with effective reaction volume and mixing. The work thus provides a process-specific modelling framework, although the present one-dimensional problem remains more simply solved by direct numerical integration, and independent validation and a matched ANN benchmark are required before claiming superior predictive performance.

2. EXPERIMENTAL AND TECHNOLOGICAL SYSTEM

2.1. HLOROGEN Units and Input Parameters

CHLOROGENH25 and CHLOROGENH1000 belong to the category of non-membrane electrolyzers. CHLOROGENH25 produces 25 g/h of active chlorine, while CHLOROGENH1000 produces 1000 g/h of active chlorine. However, the key difference between the two electrolyzers is in their geometry. Namely, HLOROGENH25 is a single-cell non-membrane tube-type electrolyzer, where the ratio of the active volume of the interelectrode space to the total volume of the electrolyzer is small. This has the effect of diluting the obtained active chlorine in the interelectrode space into the total volume of the electrolyzer. This is why an electrolyzer designed in this way cannot boast of high efficiency (the ratio of engaged power to active chlorine yield is unfavorable). On the other hand, HLOROGENH1000 is a multi-cell non-membrane electrolyzer of the cascade type, where the cells are interconnected in a cascade). The geometry of each cell is such that the ratio of the active volume of the interelectrode space to the total volume of the cell is close to unity, as a result of which the efficiency of the electrolyzer (the ratio of engaged power to the yield of active chlorine) is optimized. The aforementioned differences were the reason for their selection, to see if and to what extent NN would be able to recognize that difference.

The HLOROGENelectrolyzer has a modular design. The anodes are activated with oxides of noble and self-passivating metals, and the inlet solution contains approximately 3% NaCl. Inputs of

particular importance to the model are the concentration and pH of the brine, the type of anode coating, flow rate, geometry, current, and voltage. In addition to available chlorine, byproducts and product properties are monitored at the outlet. The PINN can therefore be developed from a demonstrative one-dimensional model into a model that includes additional physical and chemical variables.

Table 1. Declared operating data from the overview of HLOROGEN units

Unit	Capacity (kg/h)	Flow rate (L/h)	Current (A)	Voltage (V)
Hlorogen 50	0.05	5	35	3.5
Hlorogen 125	0.125	12	60	7
Hlorogen 250	0.25	25	60	14
Hlorogen 500	0.5	50	160	14
Hlorogen 1000	1.0	100	180	28
Hlorogen 2000	2.0	200	320	32

The pilot HLOROGENH25 is a tubular unit with a capacity of 2.5 L/h. The experiment used titanium anodes coated with iridium and ruthenium oxides and A4 stainless-steel cathodes. The commercial H1000 has a cascade configuration and a capacity of 100 L/h.



Figure 1. Pilot plant used in the experiment

Table 2 Characteristics of the H25 pilot electrolyzer

Parameter	Value
Anode / cathode	CFT3; A4 stainless steel
Electrode dimensions	80 × 50 mm
Number of electrodes	4 anodes; 5 cathodes
Interelectrode gap	5 mm
Total active area	320 cm²
Nominal current density	100 mA/cm²
Mean effective current density	70 mA/cm²
Theoretical current	32 A
Voltage	4 V
Brine and water dosing	electromagnetic metering pumps

2.2. Output Variables and Measurement Methods

The experiment covered residual and total chlorine concentrations, chlorite, chlorate, pH, electrolyte conductivity, oxidation–reduction potential (ORP), and residual NaCl. Available chlorine was measured by the DPD/photometric method; oxychlorine anions by liquid ion chromatography; and pH, conductivity, and ORP with a HACHHQ40d meter. Available-chlorine concentration, κ, temperature, and actual current are particularly important for linking the measurements to the model.

Table 3. Output variables monitored in the original experiment

Variable	Unit / method
Residual and total available chlorine	mg/L; DPD and UV/VIS photometry
Chlorite ClO_2^- and chlorate ClO_3^-	mg/L; ion chromatography
pH	dimensionless; HACH HQ40d
Electrolyte conductivity	µS/cm or mS/cm; HACH HQ40d
ORP	mV; HACH HQ40d

The implementation uses Python and PyTorch: torch.nn for the network and mean-squared-error loss, torch.optim.Adam for optimisation, and torch.autograd.grad for differentiation. Matplotlib produces the plots; NumPy is imported but unused. Both scripts specify a 1→100 input layer, 20 additional 100→100 layers and a 100→1 output layer, with ReLU after each of the first 21 layers. Adam uses a learning rate of 0.001 for 20000 epochs. Runtime and library versions are not recorded in the scripts, and no random seed is fixed; exact reproduction of the original training runs is therefore not established.

3. RESULTS AND DISCUSSION

3.1. Control Volume and Definitions

To derive the baseline model, the interelectrode space is treated as a tubular reactor with distributed parameters. Figure 2 shows an element of length dx, height y, and interelectrode gap z. The solution enters at volumetric flow rate F_v and molar concentration c, and leaves at concentration c + dc. The control volume is $dV = y \cdot z \cdot dx$. The baseline formulation assumes steady operation, approximately constant flow, and dominance of the principal anodic reaction.

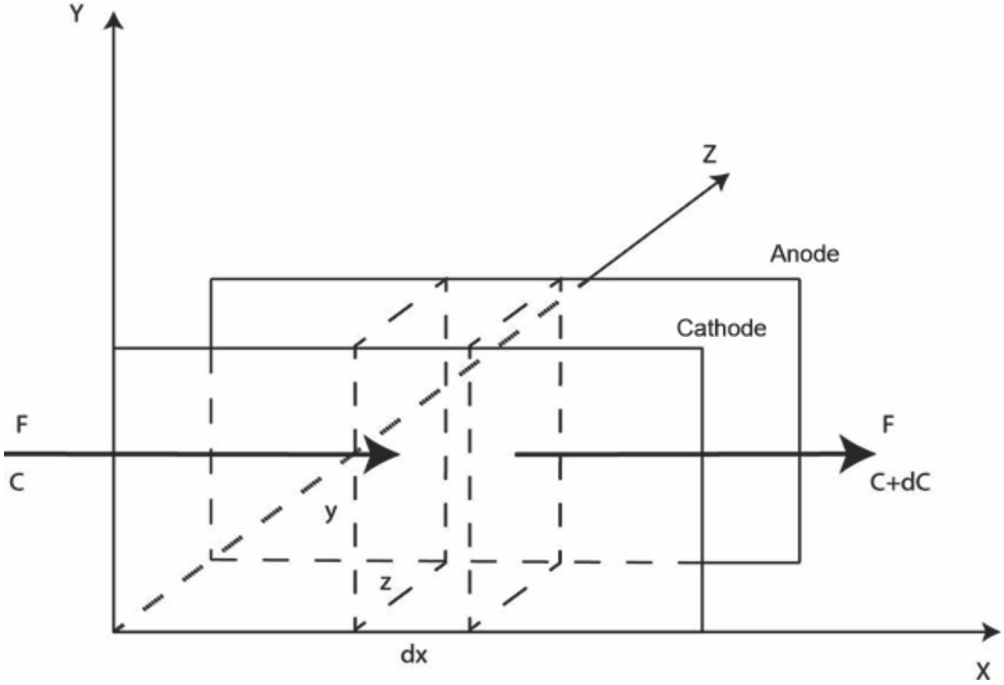


Figure 2. Control-volume schematic between the electrodes. The x, y, and z axes denote length, height, and electrode spacing. The labels F and C in the schematic correspond to volumetric flow F_v and molar concentration c in the text

At the anode, $2Cl^- \rightarrow Cl_2 + 2e^-$. For the active area of the element $(y \cdot dx)$ and current density j, the elemental current is $(dI = j \cdot y \cdot dx)$. With two electrons per Cl_2 molecule, Faraday's law gives the rate of formation, including the current-efficiency factor ξ [22]:

$$dI = j \cdot y \cdot dx$$

$$\frac{dn_{Cl_2}}{d\tau} = \frac{\xi \cdot j \cdot y \cdot dx}{2 \cdot F} \qquad (1)$$

Here F is Faraday's constant (96485 C/mol). In the ideal case, ξ = 1; in a real device, ξ accounts for yield losses due to side reactions. This addition does not change the structure of the baseline balance.

3.2. Component Balance and Steady-State Limit

For the control volume, 'accumulation = input − output + generation'. Since the outlet concentration [4] is

$c + \left(\frac{\partial c}{\partial x}\right) dx$, it follows that:

$$y \cdot z \cdot dx \cdot \frac{\partial c}{\partial t} = F_v \cdot c - F_v \left[c + \left(\frac{\partial c}{\partial x}\right) dx\right] + \frac{\xi \cdot j \cdot y}{2 \cdot F} \cdot dx \qquad (2)$$

Dividing by y z dx gives a one-dimensional transient transport equation with a local electrochemical source. Under steady-state conditions, $\frac{\partial c}{\partial t} = 0$ is assumed:

$$\frac{\partial c}{\partial t} = -\left[\frac{F_v}{y\,z}\right] \frac{\partial c}{\partial x} + \xi \frac{j}{2 \cdot F \cdot z} \qquad (3)$$

$$\frac{dc}{dx} = \xi \cdot j \cdot \frac{y}{2 \cdot F \cdot F_v} \qquad (4)$$

With the inlet condition c(0) = 0 and constant j, integration from the inlet to position x gives:

$$c(x) = \xi \cdot j \cdot y \cdot \frac{x}{2 \cdot F \cdot F_v}$$

If C is the mass concentration of available chlorine expressed as Cl_2 equivalent in g/L, and M = 0.071 kg/mol, then C[g/L] = M c[mol/m³] numerically. The baseline theoretical model is therefore:

$$C_{teor}(x) = M \cdot \xi \cdot j \cdot y \cdot \frac{x}{2 \cdot F \cdot F_v} \quad (5)$$

The same equation gives an initial design estimate of the active length required for a target outlet concentration Ciz [19]:

$$X_{teor} = 2 \cdot F \cdot F_v \cdot \frac{C_{iz}}{M \cdot \xi \cdot j \cdot y} \quad (6)$$

Equations (5) and (6) show why the baseline model is attractive: yield can be estimated quickly from flow rate, electrical loading, and geometry alone. Its limiting assumption is that j remains constant along the reactor. In a longer cascade unit, the solution changes as it passes through the system, and so do the electrical conditions between the electrodes.

3.3. Limitation of the Baseline Model and the Role of Variable Conductivity

Electrolyte conductivity κ links the electric field to local current density. For a homogeneous interelectrode layer, the ohmic resistance is approximately $R_\Omega = \frac{z}{\kappa \cdot A}$. If geometry and the effective ohmic part of the voltage remain unchanged, lower κ means lower local current density. For an electrolyte whose κ falls as C rises, the available-chlorine generation term therefore decreases downstream. The baseline model in Equation (5) still uses an initial or average j and predicts an excessively linear increase in concentration.

The terminal voltage U also includes electrode overpotentials, equilibrium potentials, and contact resistances. Consequently, the expression $j = \frac{U \cdot \kappa}{z}$ is not a complete physical law for the whole cell. A dimensionless effective factor η_{eff} can be introduced for process calculations to summarize electrical and geometric corrections. The value η_{eff} = 0.00976 in the supplied code [18] is a calibration factor for this calculation, not an independently measured current efficiency [23]:

$$j_{ef}(C) = \eta_{eff} \cdot U \cdot \frac{\kappa(C)}{z} \quad (7)$$

In the H25 pilot unit, the short active length makes the effect of changing κ relatively small. The larger discrepancy with experiment arises because the effective reaction volume between the electrodes is smaller than the vessel's total volume. The product mixes with the remaining solution after it forms. In the H1000, vessel volume better matches the active zone, making the effect of variable κ along the longer flow path more apparent/

3.5. Derivation of the Composite Conductivity Correlation

3.5.1. Aqualor H Experimental Data

The supplied Aqualor H analysis contains six measured points. C in the table is the achieved concentration, not the target value. The initial point is designated as a 3% NaCl solution, with κ_0 = 49.3 mS/cm. At C = 10.1 g/L, κ has fallen to 43.5 mS/cm, a decrease of approximately 11.8% [17].

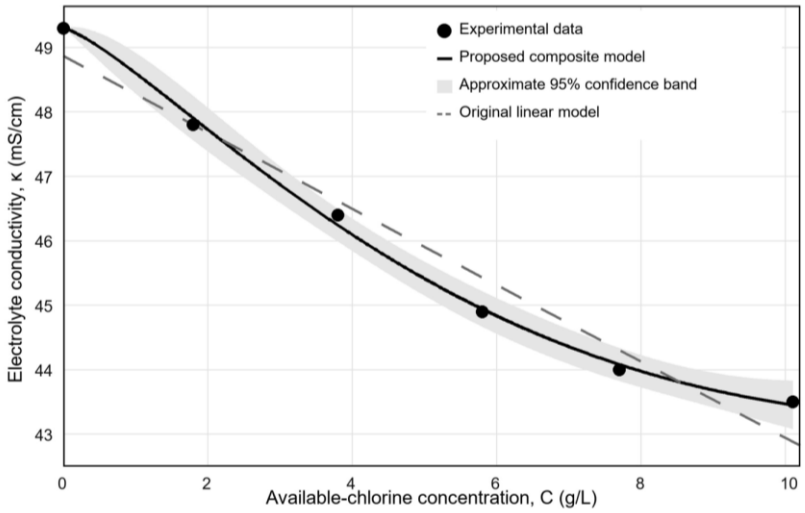


Figure 3. Measured points, composite correlation, and the original linear relation from the baseline model [17]. The gray band is an approximate confidence interval for the mean response, not a prediction interval for future measurements

Table 4. Data used to calibrate κ(C) [17]

C (g/L)	κ (mS/cm)	pH	T (°C)
0.0	49.3	6.27	17.7
1.8	47.8	9.34	16.3
3.8	46.4	9.53	16.3
5.8	44.9	9.58	15.3
7.7	44.0	9.60	15.5
10.1	43.5	9.64	14.2

3.6. From the Literature to a Process Equation

Electrolyte conductivity depends on the number of mobile ions and their mobility: $(\kappa = \Sigma_i n_i \cdot |q_i| \cdot \mu_i)$. Zhang et al. [19] proposed a semiempirical structure in which the number of free ions follows a power law in electrolyte concentration m while mobility declines approximately exponentially; their combination has the form $(\kappa = A \cdot m^n \cdot e^{-B \cdot m})$. Molecular approaches by Gering [20]and by Zhang, Bier, and Viswanathan [21] further explain the effects of solvation, ion pairing, and solution structure. Not all inputs needed for such a fully molecular model are available for Aqualor H.

Available chlorine C is not the total electrolyte concentration: at C = 0, the initial brine already conducts well. The form reported in the literature is therefore not applied directly to κ(C), which would incorrectly imply κ(0) = 0. Instead, the change relative to the initial value is modeled. This is a process-level adaptation of the functional form, not microscopic proof of a mechanism in the NaCl/NaOCl mixture [21]:

$$\Delta\kappa(C) = \kappa_0 - \kappa(C) = A \cdot C^n \cdot e^{-B \cdot C} \qquad (8)$$

The coefficients A, n, and B were estimated by nonlinear least squares from the six measurements, with κ_0 fixed at 49.3 mS/cm. The resulting values are A = 0.77148, n = 1.32200, and B = 0.10216 L/g. The recommended correlation is [21]:

$$\kappa(C) = 49.300 - 0.77148 \cdot C^{1.322} e^{-0.10216 \cdot C} \quad [mS/cm] \qquad (9)$$

To use κ in the current-density equation, the value in mS/cm must be divided by 10 to obtain S/m. The correlation was calibrated only over 0 ≤ C ≤ 10.1 g/L. Its monotonic branch ends mathematically at approximately C = n/B = 12.94 g/L, but extrapolation even to that point is not justified without new data.

3.7. Improvement in Data Fit and Limits of Identification

For the same six points, the composite correlation gives $R^2 = 0.99823$ and RMSE = 0.0873 mS/cm. The original linear expression $\kappa_{lin}(C) = 48.867 - 0.5926\ C$ gives $R^2 = 0.96158$ and RMSE = 0.4060 mS/cm [16, 17]. At C = 10.1 g/L, the linear expression predicts 42.882 mS/cm and the new equation predicts 43.453 mS/cm, compared with a measured 43.500 mS/cm. A better fit does not, by itself, constitute independent predictive validation: only six points, with no reported replicates, were used to estimate three parameters.

Temperature decreased simultaneously from 17.7 to 14.2 °C; the reported correlation between C and T is r = −0.948 [17]. These points cannot separately identify the effects of temperature and changing ionic composition. In addition, the report text refers to dilution of the product with demineralized water, whereas its table identifies the C = 0 point as the initial 3% brine. The preparation procedure should therefore be clarified in the next measurement campaign. Equation (9) is a calibrated process correlation for the data described, not a universal function for all available-chlorine solutions.

3.8. Combining the Balance and Correlation in the Enhanced Model

Substituting the local current density from (7) into Faraday's balance and writing it in terms of mass concentration yields the equation used by the later PINN code. Its effective factor also includes corrections that have not been identified separately; it should not be multiplied by an additional unknown ξ without recalibration [19]:

$$\frac{dC}{dx} = \left[M \cdot \eta_{eff} \cdot U \cdot \frac{y}{2 \cdot F \cdot F_v \cdot z}\right] \cdot \kappa(C), \quad C(0) = 0 \qquad (10)$$

For a target outlet concentration Ciz, variable conductivity must be integrated along the profile rather than replaced everywhere by its outlet value [21]:

$$x(C_{iz}) = [2 \cdot F \cdot F_v \cdot z/(M \cdot \eta_{eff} \cdot U \cdot y)] \cdot \int_0^{C_{iz}} \frac{dc}{\kappa(c)} \qquad (11)$$

For the input parameters $F_v = 2.78 \times 10^{-5}$ m³/s, U = 30 V, y = 0.2 m, z = 0.003 m, M = 0.071 kg/mol, and $\eta_{eff} = 0.00976$, numerical integration of (10) gives C(8 m) ≈ 9.48 g/L. For the same input conditions, the baseline model (5), with j = 477 A/m² and ξ = 1, gives 10.10 g/L.

3.9. Development of the PINN

3.9.1. Principle of the Approach

A physics-informed neural network (PINN) represents the unknown function Ĉθ(x), where θ denotes the trainable network parameters. Position x is the input, and predicted concentration is the output. Automatic differentiation computes dĈθ/dx at selected points along the active length. The derivative is then compared with the right-hand side of model (10). The network is trained to satisfy both the differential equation and the inlet condition. It is therefore more than a black box reproducing an experimental curve: the physical balance constrains the admissible shape of its output.

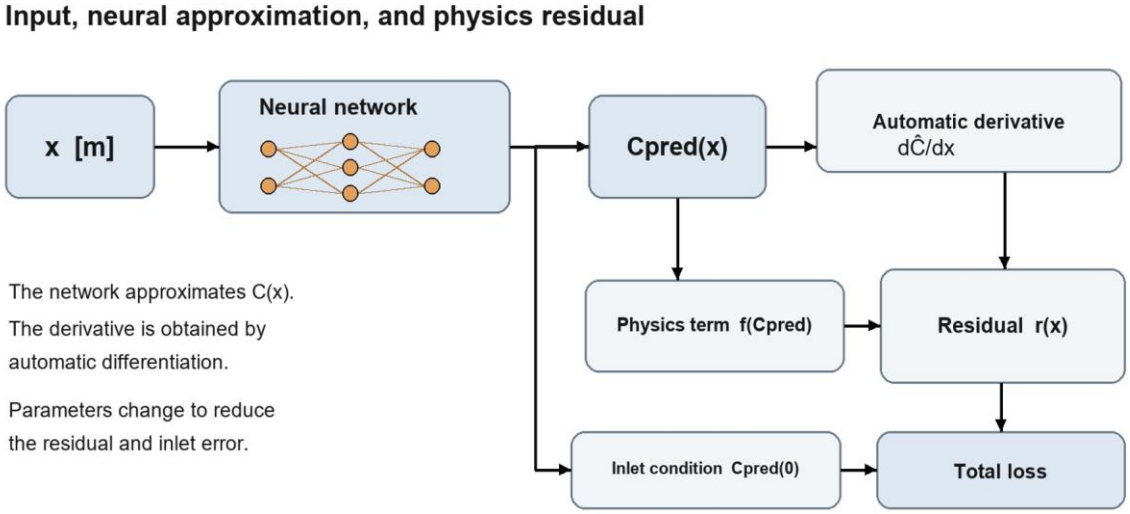


Figure 4. Schematic of the PINN procedure

For a set of interior points x_i, the residual and the loss-function terms can be written as [22]:

$$r\theta(x_i) = \frac{d\hat{C}\theta}{dx} - \left[M\,\eta_{eff}\,U\frac{y}{2F\,F_v\,z}\right]\kappa\left(\hat{C}\theta(x_i)\right) \quad (12)$$

$$Lphys = (1/N)\,\Sigma_i\, r\theta(x_i)^2;$$
$$LBC = [\hat{C}\theta(0) - C_0]^2$$
$$L = Lphys + LBC \quad (13)$$

The optimizer adjusts θ to reduce L. If needed, a data-fit term can also be added: $L_{data} = \left(\frac{1}{N_d}\right)\Sigma\left[\hat{C}\theta(x_k) - C_0\right]^2$

This term is not active in the supplied code. Therefore, the visual agreement between the PINN profile and C_data does not demonstrate that the network learned from those points. It primarily tests how well the chosen physics, coefficients, and inlet condition reproduce the observed profile.

3.10. PINN Architecture

The PINN has 20 hidden layers with 100 neurons each, ReLU activations, an Adam optimizer with a learning rate of 0.001, and 20,000 training epochs.

For the present one-dimensional steady-state equation, direct integration is simpler and provides a reliable check on the PINN solution. The value of the PINN approach increases when the model is extended to a variable temperature field, nonuniform current density, cascade geometry, transport, and chemical side reactions, or when limited data are combined with known laws. Each extension nevertheless requires new measurements and independent validation.

3.11. Results for the H25 Pilot Unit

Figure 5 Results of the H25 pilot PINN analysis: (a) concentration profiles from the theoretical model, PINN, and experiment; (b) training-loss history.

Over the short active length of the H25, the PINN and theoretical-model profiles are close, whereas the experimental concentrations are lower. This does not mean the PINN failed: it satisfies the physics it was given. The discrepancy with measurements indicates that an important part of the device was omitted from the physical description. The main cause is the ratio between the effective reaction volume in the interelectrode space and the total electrolytic-vessel volume; subsequent mixing dilutes the available chlorine formed. With a short electrode, the variation of κ along the path has a smaller effect, so adding it alone does not close this gap.

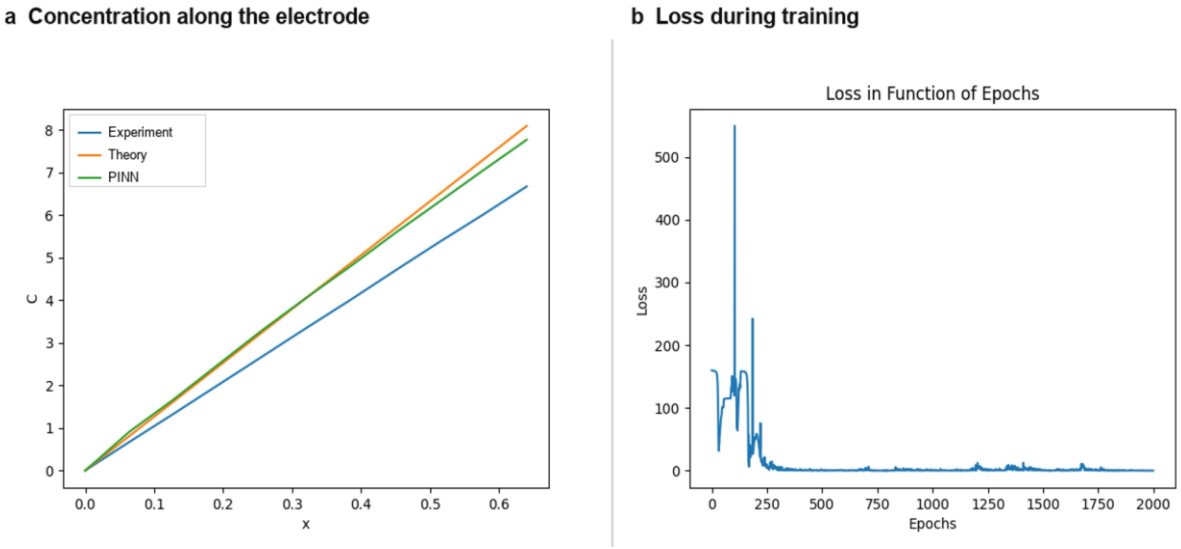


Figure 5. Results of the H25 pilot PINN analysis: (a) concentration profiles from the theoretical model, PINN, and experiment; (b) training-loss history

In Figure 5b, the loss falls sharply during training. A low loss confirms consistency with the specified equation and inlet condition, but it does not directly measure deviation from laboratory data, because those data are not included in the plotted loss.

3.12. Results for the H1000 Cascade Unit

Figure 6 Results of the H1000PINN analysis: (a) theoretical, PINN, and experimental concentration profiles; (b) training-loss history.

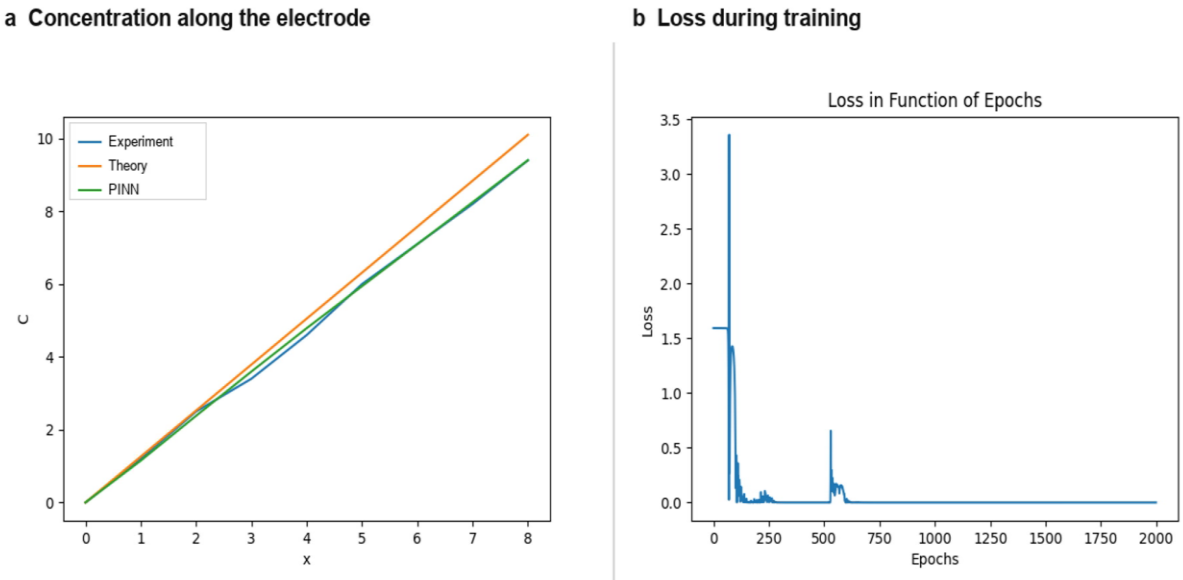


Figure 6. Results of the H1000PINN analysis: (a) theoretical, PINN, and experimental concentration profiles; (b) training-loss history

Over the longer active path of the H1000, the theoretical profile with constant current density ends above the experimental profile, while the plotted PINN profile approaches the measured curve. The main cause of this difference is the decline in electrolyte conductivity as available chlorine forms, which reduces local current and the production rate in downstream sections. Unlike the pilot device, the cascade configuration makes the total volume closer to the effective reaction volume, so additional dilution is less important.

Table 5. Comparison of outlet concentrations for an illustrative H1000 parameter set

Approach	C at x = 8 m (g/L)	Status
Baseline model, constant j = 477 A/m²	10.10	Calculated from (5)
Enhanced Equation (10), numerical integration	9.48	Calculated from κ(C) and η_{eff}
PINN profile	About 9.4–9.5	Read from an earlier plot; linear κ

3.13. PINN Contributions and Outstanding Validation

The PINN's principal contribution in this work is to combine available physical knowledge in a numerical model that can be extended. It gives concentration as a function of position, tests whether the selected equation can satisfy the inlet condition, and permits additional residual terms as new phenomena are identified. The H25–H1000 comparison also illustrates its diagnostic value: different patterns of disagreement with experiment point to different missing effects, particularly mixing and vessel volume in the pilot unit and changing electrical conditions along the cascade.

A low training loss is no substitute for validation. The next step is to measure C, κ, temperature, current, and voltage by electrolyzer section; repeat the conductivity measurements at controlled temperatures; and reserve a separate series for validation. For the H25, the ratio of active to total volume should be quantified; for the H1000, the current distribution and ηeff should be checked.

As for limited number of experimental oints, the limitations of such a data set and its potential impact on the reliability of the proposed model should be discussed.

Namely, the conductivity–concentration relationship was calibrated using only six experimental points, which limits the statistical strength and generalizability of the proposed model. With three fitted coefficients and a fixed initial conductivity, only three residual degrees of freedom remain; consequently, the high coefficient of determination primarily demonstrates agreement with the calibration data and does not establish predictive reliability. Individual measurements may strongly influence the estimated parameters, while the absence of reported replicate measurements prevents an independent assessment of experimental variability. Moreover, temperature decreased simultaneously with increasing available-chlorine concentration, so the present data cannot distinguish temperature effects from changes in electrolyte composition. The proposed relationship should therefore be regarded as a preliminary process-specific correlation within the investigated range of 0–10.1 g/L, with extrapolation beyond this range avoided. Further validation requires additional measurements distributed across the concentration range, replicate experiments at controlled temperatures, and an independent data set for evaluating prediction errors and uncertainty.

The robustness of the proposed framework depends on both the experimental calibration of the conductivity relationship and the numerical training of the PINN. In the present study, six experimental conductivity–concentration pairs were used to estimate three coefficients, with the initial conductivity fixed. These measurements were used for calibration rather than divided into separate training and validation subsets, and consequently do not provide independent evidence of predictive accuracy. The PINN was trained through the governing-equation residual and inlet-condition constraint; experimental concentration measure-ments were not included directly in its loss function. Thus, the principal risk associated with the small experimental data set is overfitting of the conductivity correlation and sensitivity of its coefficients to individual observations, rather than conventional supervised overfitting of the PINN to six measurements.

A substantially larger experimental data set, distributed across the concentration range and including replicate measurements at controlled temperatures, would permit more reliable parameter estimation, assessment of experimental variability, and reservation of independent measurements for validation. Measurements obtained under different flow rates and electrical operating conditions would additionally test whether the coupled model remains reliable beyond its calibration conditions. However, additional data alone cannot compensate for omitted physical mechanisms or systematic measurement errors. Numerical robustness should also be assessed by repeating PINN training with different random initializations and comparing its predictions with direct numerical integration of the same governing equation.

4. CONCLUSION

The baseline Faraday model provides a transparent theoretical foundation, but constant j tends to overestimate outlet yield when conductivity decreases along the cascade electrolyzer. The Aqualor H composite correlation introduces the measured variation κ(C), with a clear restriction to its calibrated range. The PINN incorporates this physics into training through the differential-equation residual and inlet condition. The presented results explain why theory, PINN, and experiment agree more closely for the H1000 when variable conductivity is included, and why a discrepancy remains for the H25 because of geometry and mixing. The AI approach offers a way to connect physical laws with data and extend the model systematically; its ultimate accuracy depends on the completeness of the physical description and independent experimental validation.

Acknowledgement

The authors would like to acknowledge the supported by the Ministry of Education, Science and Technological Development of the Republic of Serbia (Contract No. 451-03-33/2026-03/200053).

This work was supported by COST Action CA25106 STILLNESS, under the European Cooperation in Science and Tehnology (COST).

Appendix A Symbols

Table A1 Symbols used in the model

Symbol	Meaning and unit
C, c	Mass concentration (g/L) and molar concentration (mol/m³) of available chlorine as Cl_2 equivalent
F_v, F	Volumetric flow rate (m³/s) and Faraday's constant (C/mol)
M, j	Molar mass of Cl_2 (kg/mol) and effective current density (A/m²)
κ, $κ_0$	Electrolyte conductivity and its initial value (mS/cm or S/m)
x, y, z	Position / length, electrode height, and interelectrode gap (m)
U, ξ, ηeff	Voltage (V), current efficiency, and effective process factor
Ĉθ, θ	Concentration approximated by the PINN and neural-network parameters

5. REFERENCES

[1] J. Newman, K. E. Thomas-Alyea (2004) Electrochemical Systems, 3rd ed., Wiley-Interscience, Hoboken, NJ, USA.

[2] A. J. Bard, L. R. Faulkner (2001) Electrochemical Methods: Fundamentals and Applications, 2nd ed., Wiley, New York.

[3] T. F. O'Brien, T. V. Bommaraju, F. Hine (2005) Handbook of Chlor-Alkali Technology, Springer.

[4] D. Pletcher, F. C. Walsh (1990) Industrial Electrochemistry, 2nd ed., Chapman & Hall.

[5] Black & Veatch Corporation (2010) White's Handbook of Chlorination and Alternative Disinfectants, 5th ed., Wiley, Hoboken, NJ, USA.

[6] H. B. Beer (1980) The invention and industrial development of dimensionally stable anodes, Journal of the Electrochemical Society, 127, 303C–307C.

[7] S. Trasatti (1987) Electrocatalysis in the anodic evolution of oxygen and chlorine, Electrochimica Acta, 32, 369–382.

[8] J. Jeong, C. Kim, J. Yoon (2009) The effect of electrode material on the generation of oxidants and microbial inactivation in electrochemical disinfection processes, Water Research, 43, 895–901. https://doi.org/10.1016/j.watres.2008.11.033

[9] A. Kraft (2008) Electrochemical water disinfection: A short review, Platinum Metals Review, 52, 177–185. https://doi.org/10.1595/147106708X329273

[10] D. Ghernaout, M. W. Naceur (2011) Ferrate(VI): In situ generation and water treatment—A review, Desalination and Water Treatment, 30, 319–332. https://doi.org/10.5004/dwt.2011.2217

[11] X. Chen, G. Chen, P. L. Yue (2000) Separation of pollutants from restaurant wastewater by electrocoagulation, Separation and Purification Technology, 19, 65–76.

[12] C. A. Martínez-Huitle, E. Brillas (2009) Decontamination of wastewaters containing synthetic organic dyes by electrochemical methods. A general review, Applied Catalysis B: Environmental, 87, 105–145. https://doi.org/10.1016/j.apcatb.2008.09.017

[13] C. Comninellis (1994) Electrocatalysis in the electrochemical conversion/combustion of organic pollutants for wastewater treatment, Electrochimica Acta, 39, 1857–1862.

[14] C. Comninellis, G. Chen (Eds.) (2010) Electrochemistry for the Environment, Springer

[15] J. C. Morris (1966) The acid ionization constant of HOCl from 5 to 35°C, Journal of Physical Chemistry, 70, 3798–3805.

[16] S. Kolić, M. Džomba, M. N. KrstajićPajić (2024) HLOROGEN – In Situ Electrochemical Production of Available Chlorine: Characteristics and Optimization, 9th Regional Symposium on Electrochemistry – South-East Europe, Novi Sad, Serbia, June 3–7, p. 21.

[17] HLOROGEN development documentation (2026) Semiempirical Model of the Dependence of Aqualor H Conductivity on Available-Chlorine Concentration: Proposed Equation, Theoretical Rationale, and Statistical Validation, Predlog_ modela_ elektro-provodljivosti_Aqualor_H_Korigovan", 22 June.

[18] HLOROGEN development documentation (2026) Electrolysis PINNOptimiser – H1000.

[19] W. Zhang, X. Chen, Y. Wang, L. Wu, Y. Hu (2020) Experimental and Modeling of Conductivity for Electrolyte Solution Systems, ACS Omega, 5, 22465–22474. https://doi.org/10.1021/acsomega.0c03013

[20] K. L. Gering (2017) Prediction of Electrolyte Conductivity: Results from a Generalized Molecular Model Based on Ion Solvation and a Chemical Physics Framework, ElectrochimicaActa, 225, 175–189. https://doi.org/10.1016/j.electacta.2016.12.083

[21] Y. Zhang, I. Bier, V. Viswanathan (2022) Predicting Electrolyte Conductivity Directly from Molecular-Level Interactions, ACS Energy Letters, 7, 4061–4070. https://doi.org/10.1021/acsenergylett.2c01947

[22] E. M. Raissi, P. Perdikaris, G. E. Karniadakis (2019) Physics-informed neural networks: A deep learning framework for solving forward and inverse problems involving nonlinear partial differential equations, Journal of Computational Physics, 378, 686–707. https://doi.org/10.1016/j.jcp.2018.10.045.

[23] F. Gamry Instruments, Electrolyte Resistance, technical documentation. https://www.gamry.com/support-2/

IZVOD

PRIMENA NEURONSKE MREŽE ZASNOVANE NA FIZIČKIM ZAKONIMA ZA OPTIMIZACIJU PROIZVODNJE HLORA PUTEM ELEKTROLIZE BEZ MEMBRANE

*U ovom radu prikazano je kako neuronska mreža zasnovana na fizičkim zakonima (engl. *physics-informed neural network* – PINN) može da poveže Faradejev zakon, promenljivu provodljivost elektrolita i eksperimentalne podatke u okviru modela proizvodnje aktivnog hlora. Najpre, bilans komponenti u stacionarnom stanju daje polaznu linearnu vezu između koncentracije i aktivne dužine elektrode. Zatim se pokazuje zašto pretpostavka o konstantnoj gustini struje dovodi do precenjivanja izlazne koncentracije u kaskadnom elektrolizeru veće dužine: provodljivost elektrolita opada tokom procesa konverzije. Na osnovu šest merenja sprovedenih na uređaju „Aqualor H" izvedena je korelacija k(C) = 49,300 - 0,77148·C^1,322·e^(-0,10216·C), inspirisana poluempirijskim modelima koncentracije i pokretljivosti slobodnih jona. PINN aproksimira prostorni profil koncentracije, a proces učenja se odvija putem smanjenja reziduala diferencijalne jednačine i greške u odnosu na ulazne uslove. Grafički prikazi pokazuju približno slaganje između rezultata dobijenih pomoću PINN-a i teorijskog modela za kraći pilot-elektrolizer H25, dok je eksperimentalni prinos niži usled uticaja zapremine reaktora. Za model H1000, PINN preciznije prati eksperimentalni profil nego teorijski model sa konstantnom gustinom struje. Unapređeni model koristi kombinovanu korelaciju za provodljivost; numeričko rešavanje odgovarajuće jednačine daje izlaznu koncentraciju od oko 9,48 g/L za usvojene parametre, u poređenju sa 10,10 g/L prema polaznom modelu i 9,4 g/L u prikazanoj eksperimentalnoj seriji.*

Ključne reči: *PINN; veštačka inteligencija; aktivni hlor; elektroliza bez membrane; Faradejev zakon; provodljivost elektrolita; Aqualor H.*

Naučni rad
Rad primljen: 22.10.2026.
Rad prihvaćen: 28.10.2026.

https://orcid.org/0000-0002-3208-016X – Marija Mitrovic,

https://orcid.org/0000-0002-8860-4890 – Nevenka Elezovic,

© 2026 Authors. Published by Engineering Society for Corrosion. This article is an open access article distributed under the terms and conditions of the Creative Commons Attribution 4.0 International license (https://creativecommons.org/licenses/by/4.0/